Performance of Poly(ethylene-*co*-vinyl acetate) Nanocomposites Using Distinct Clays

Vinicios Pistor,[1] Heitor Luiz Ornaghi Jr.,[2] Carlos Arthur Ferreira,[2] Ademir José Zattera[1]

[1]*LPOL/Universidade de Caxias do Sul, Caxias do Sul, RS, Brazil*
[2]*PPGEM/Universidade Federal do Rio Grande do Sul, Porto Alegre, RS, Brazil*

Received 16 August 2010; accepted 16 January 2011
DOI 10.1002/app.34804
Published online 29 January 2012 in Wiley Online Library (wileyonlinelibrary.com).

ABSTRACT: This study aimed to evaluate the performance of EVA nanocomposites with distinct clays. Three different types of nanoclays were used (Na^+, 15A, and 30B) at a processing speed of 400 rpm. By DMA, an increase in the storage and loss moduli was found, as well as lower peak height and peak width at half-height for the nanocomposites containing 15A clay. Also, in rheometry analysis, higher moduli values were obtained for the 15A clay nanocomposite. The relaxation and retardation spectra showed three distinct peaks for the nanocomposites containing the organophilic clays. Finally, the XRD and TEM analysis showed a microcomposite formation, intercalated and exfoliated structure for the Na^+, 15A, and 30B nanocomposites, respectively. These results possibility a greater understanding of the interaction effects between the intercalated (15A) and exfoliated (30B) clays and the influence of the type of modifier in the nanocomposites studied. © 2012 Wiley Periodicals, Inc. J Appl Polym Sci 125: E462–E470, 2012

Key words: nanocomposites; viscoelasticity; physical interactions; relaxation and retardation functions

INTRODUCTION

Nanocomposites obtained by the incorporation of nanoclays into thermoplastic polymeric matrices have been the subject of several recent studies, and they can be used for different applications. According to Ray and Okamoto,[1] hydrated silicate layers with ions (usually Na^+ or K^+) in nanoclays are miscible only with hydrophilic polymeric matrices. The same authors reported that the miscibility of these nanofillers with other polymeric matrices can be obtained by first converting them to organophilic matrices.

The use of surfactants containing distinct contents of alkyl chains[2] and polar tensoactives[3] enables the attainment of modified clays.[3]

Marini et al.[4] reports that nanoclays modified with polar tensoactives make the exfoliation with polar polymers more efficient, due to the more suitable processing conditions. However, many authors have studied poly(ethylene-*co*-acetate) matrices formed of clays with distinct segments and alkyl chain lengths.[5–7]

Zhang et al.[5] studied the incorporation of different clays containing long segments of alkyl chains in an EVA matrix and reported that, generally, the higher polarity of the polymeric chains and higher basal spacing of the clay makes it easier to obtain exfoliated structures.

La Mantia and Dintcheva,[6] for dispersed nanoclays processed in a twin screw extruder, noted an increase in viscosity and a non-Newtonian behavior attributed to the good dispersion and greater strain-hardening effect in an isothermal elongational flow in relation to the pure EVA matrix.

Chaudhary et al.,[7] studying the incorporation of organophilic clays 15A and 30B in an EVA matrix, reported that the modified clay 15A is the best alternative when a hydrophobic polymer (like EVA) is used. The long aliphatic chains of the acetate vinyl content of the EVA matrix lead to a better attraction between the galleries of the clays and the polymeric chains. In addition, the modified nanoclay 30B has bis-(2-hydroxyethyl) tallow in its structure, leading to better interaction with hydrophilic polymers.

The main objective of this study was to analyze the physical interactions that can be associated with the dispersion of the clays Cloisite® 15A (with long aliphatic chains) and Cloisite® 30B (with hydroxyl terminals), both incorporated into an EVA matrix containing 28% (w/w) of vinyl acetate (VAc) in a corotating twin-screw extruder.

EXPERIMENTAL

Materials

The materials used in this study were: poly (ethylene-*co*-vinyl acetate) (EVA) (UE-2824/32) containing 28% of vinyl acetate (VAc), supplied by Polietilenos

Correspondence to: V. Pistor (pistorv@yahoo.com) or A. J. Zattera (ajzatter@ucs.br).

Contract grant sponsor: UCS, UFRGS, CNPq, CAPES, FAPERGS.

União S/A, the natural organophobic clay (Cloisite® Na^+) and organophilic modified montmorillonite (OMMT) clay with quaternary ammonium salt containing chain segments with ~ 65% C18; ~ 30% C16; ~ 5% C14 (Cloisite® 15A; dimethyl, dehydrogenated tallow, quaternary ammonium) and OMMT clay with two hydroxyl terminals (Cloisite® 30B; methyl, tallow, bis-2-hydroxyethyl, quaternary ammonium), supplied by Southern Clay Products.

EVA nanocomposites containing five parts per hundred (phr) of clay (Na^+, 15A, or 30B) were prepared. After drying the clays in an oven with air circulation at a temperature of 60°C for 8 h, the nanocomposites were processed in a molten mixture process using a corotating twin screw extruder (MH-COR-20-32-LAB, MH Equipment; $D = 20$ mm, $L/D = 32$) with eight heating zones and temperature profiles (100, 120, 140, 160, 130*, 160, 160, and 160°C—barrel to matrix, respectively). The speed processing of 400 rpm was used to process the nanocomposites. In zone 5* degassing with the aid of a vacuum was used for the elimination of volatiles.

Characterization of the nanocomposites

The X-ray diffractograms were collected with a sample holder mounted on a Shimadzu diffractometer (XRD-6000), with monochromatic Cu Kα radiation ($\lambda = 0.15418$ nm) and the generator working at 40 kV and 30 mA. Intensities were measured in the range of $1° < 2\theta < 12°$, typically with scan steps of 0.05° and 2 s $step^{-1}$ (1.5° min^{-1}).

The viscoelastic properties of the nanocomposites in the solid state were determined using a Dynamic Mechanical Analyzer (DMA 2980). Tests were performed at the frequency of 1 Hz and heated from −130 to 60°C using a heating rate of 3°C min^{-1} and the analysis was carried out in dual cantilever mode at a strain amplitude of 10 μm.

The samples were analyzed in an Anton Paar oscillatory rheometer (Physica MCR 101), with parallel plates of 25 mm diameter and a gap between the plates of 1 mm, test temperature of 160°C, frequency range of 0.1–100 Hz, shear stress of 200 Pa and nitrogen flow of 1 m^3 h^{-1}. From the rheological analysis, the relaxation ($H(t)$) spectra were collected using a nonlinear regression (NLREG) program.[8–10]

The samples were prepared using cryo-ultramicrotomy. They were mounted on cryo-pins and frozen in liquid nitrogen. The experiments were performed using a JEOL transmission electronic microscopic, model JEM 1200 EX II, at 80 kV.

RESULTS AND DISCUSSION

X-ray diffraction (XRD)

X-ray diffractograms were obtained for the nonprocessed nanoclays and the nanocomposites (including the EVA matrix) processed at 400 rpm. Also, the nonmodified sodium clay (Na^+) was added to allow a direct comparison with the respective modified 15A and 30B nanoclays. Figure 1 show the XRD patterns for the neat resin, nanoclays and for the nanocomposites studied.

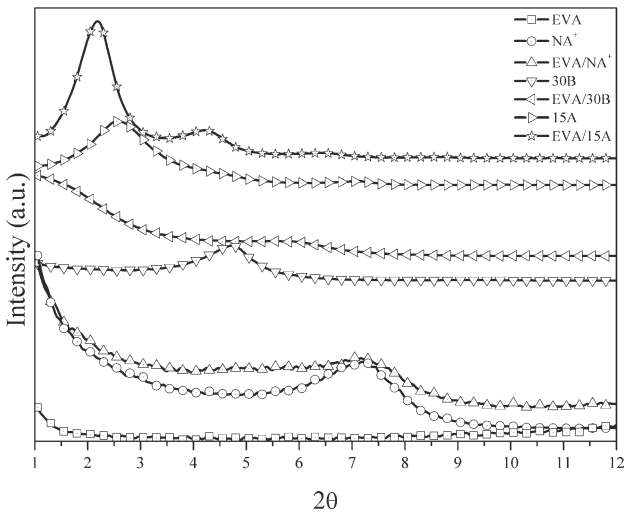

Figure 1 X-Ray diffractograms obtained for the neat EVA, nanoclays and the nanocomposites containing Na^+, 15A, and 30B clays.

The broadening of the curve (when incorporated the Na^+ in the matrix) represents the distribution of the clay in the matrix. The incorporation of this clay reduces the radiation incidence in the X-ray region and inhibits the response of the incidence by shifting the electrons that reflect the crystalline plane of the clay. As a result, the dispersion of the clay in the EVA matrix becomes evident.

The 15A nanoclay shows a diffraction peak at $2\theta \approx 2.5°$. With incorporation of the clay 15A in the matrix, it is clear a defragmentation of this diffraction peak into two other distinct and well defined peaks ($2\theta \approx 2°$ and 4.5°, referring to the planes (001) and (002)). Even, a third peak (lower and difficult to visualize), occurs ($2\theta \approx 6.5°$, referred to the plane (003)).[7]

Chaudhary et al.[7] describe that in relation to the organophilic clay 15A, the silicate layers expand themselves due the intercalation of the polymer chains between the gallery spaces. Consequently, the diffraction peak becomes very broad and less intense; which suggests the possibility of a disordered intercalated structure.

It can be noted that the diffraction peak of the Na^+ clay is situated at $2\theta = 7$, corresponding to the crystalline plane (001). The peak diffraction of 30B ($2\theta = 4.75°$),[7] demonstrates the same behavior as the dispersion of the Na^+ clay. According to Gupta et al.,[11] reductions in the intensity and the width of the diffraction peak are indicative of a higher basal

spacing of the clays and thus of an exfoliated morphology.

Dynamic mechanical analysis

There are distinct relaxation processes for the EVA polymer corresponding to the crystalline phase (comprised of polymethylenic units), an interfacial region (with both ethylenic and VAc segments) and a complex amorphous phase (with noncrystallized methylenic segments and VAc units). These relaxation processes are observed through the respective transitions: γ, β, and α. They are related to the methylenic units, VAc segment, and the main transition.

The storage moduli were calculated as a function of temperature for all analyses. According to Figure 2, it is clear that for EVA and EVA/30B samples, in the glassy region there was an increase in the moduli values at around −75°C. First, this could be attributed to the β transition (transition associated with the interfacial region between the amorphous and crystalline phases).[12] This is not reasonable due an increase in the modulus. In the main and secondary transitions, (when observed the storage modulus) there is a decreasing in the storage modulus due the molecular motion. So, can be occurring an orientation of the ester-side groups, which promotes rigidity in the EVA matrix chains. Besides, there is a polarization that causes a molecular orientation of the EVA chains and consequently an increase in the storage modulus in the glassy region.

As the temperature increases, a fall is observed in the onset temperature of the glass transition region, which extends into the elastomeric region. However, in the glassy transition region, the samples show differences attributed to the incorporation of the nanofillers, which promote a stiffer system. In general, for composites and nanocomposites, the reinforcement is more effective when passing through the glass transition region.[13] In the elastomeric region, there is a less abrupt fall in the temperature related to the glassy region for more reinforced materials.[14] In a semicrystalline polymer, the glass transition temperature is related to the amorphous content[15]; however, the incorporation of nanofiller decreases the quantity of crystalline content, which initially should promote a softening in the system, but the incorporation of a stiff component leads to greater restriction in the molecular movement, shifting this transition to higher temperatures. Another aspect that should be noted is that if the system is exfoliated, the quantity of amorphous phase will increase. With the incorporation of the 15A clay there is stiffness in the system, increasing the enthalpy factor and decreasing the entropy factor. This is associated with higher energy being needed to begin the molecular motion.[16] The rigidity of the system is attributed with the quantity of strong bonds; however, since there is no interaction between the components, the increase in the free volume leads to greater flexibility. Flexibility is associated with segment movement, chain stiffness or steric hindrance and free volume.[15]

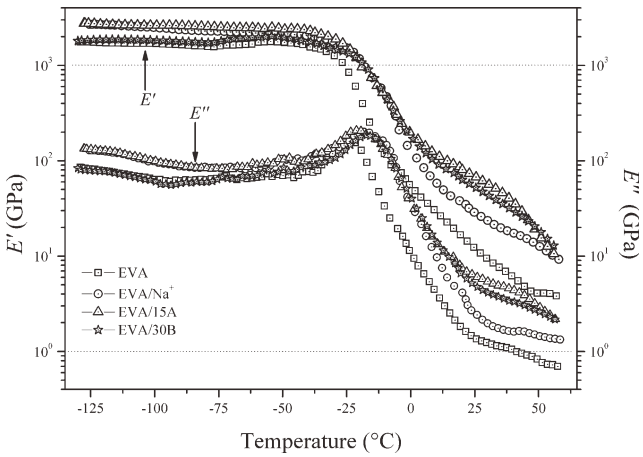

Figure 2 Storage (E') and loss (E'') moduli for the neat EVA and the nanocomposites studied.

Also, it can be observed (for loss modulus) that there is an increase in the dissipation energy for the 15A sample. This higher energy dissipation is attributed to the long aliphatic chains of the nanofiller that occupy a greater amount of free volume when sufficient thermal energy is obtained for the long segmental distances. Besides, there is higher free volume between the chains and consequently dissipation of more energy. Lower energy dissipation was noted for the EVA matrix. In general, higher energy dissipation is attributed to the matrix[17] however; in this case, with the presence of the nanofillers there is an interface that is not present in the pure matrix. In principle, this interface will provide a higher contact area and lead to a more flexible system through the motion of the chain segment containing the reinforcement.[18]

As can be seen in Figure 3, it is possible to note that the glass transition temperature was lower for the EVA sample in relation to the other nanocomposites studied. Higher mobility was observed for the pure matrix, as seen in the loss modulus and, as the restriction to the molecular mobility is increased, higher thermal energy is needed to initiate the molecular segmental motion.[13] Besides T_g, from the tan delta curves were obtained the peak height and peak width at half-height for the neat EVA and all nanocomposites studied.

From the tan delta results in Table I it can be noted that there is a lower peak width at half-height for the 15A sample, initially indicating a more homogeneous system due to the obtainment of a more exfoliated system. This homogeneity leads to a

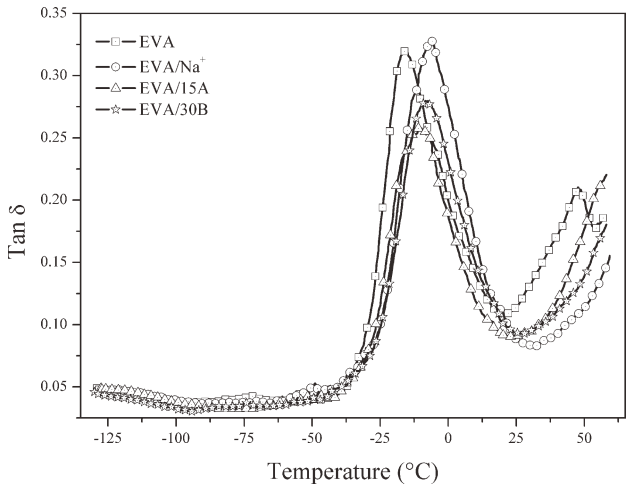

Figure 3 Damping factor (tan δ) obtained for the neat EVA and the nanocomposites studied.

narrower distribution of relaxation times as seen in earlier studies.[19,20] When the distribution of the relaxation times is very broad, this indicates the presence of short and long segments that relax at different times.[21]

The peak height shows lower values for the 15A sample which, in principle, can be attributed to a higher degree of stress being transferred to the nanofillers by the matrix.[18] If the reinforcement is effective, lower energy dissipation will occur. Higher values are usually obtained for the matrix; however, an increase in this property can be attributed to a more exfoliated system having a greater contact area due to a better distribution of the nanofillers promoting higher interplanar distances. The structure formed in an exfoliated system promotes a greater quantity of nanoclay distributed in a more uniform manner. Each "little" agglomerate formed is able to dissipate more energy due the presence of long aliphatic chains (in the case of the 15A nanofiller) and since each agglomerate receives the tension at the same (or very similar) time through the interface, there is an increase in the dissipation energy due to the higher mobility of the system.

The Cole–Cole method is a dielectric relaxation method used to describe the homogeneity of the system through the format of a characteristic semicircle.

TABLE I
Parameters Obtained Through Tan δ in the DMA Analysis

Sample	Peak Width at half-height	Peak height	T_g (°C)
EVA	0.31	0.25	−16.62
EVA/Na^+	0.33	0.26	−5.89
EVA/15A	0.25	0.19	−11.39
EVA/30B	0.28	0.21	−8.21

A more closed semicircle is attributed to the segments relaxing at similar times in contrast to a broad semicircle that reflects a larger distribution of relaxation times.[22] Considering the time-temperature equivalence,[16] Cole–Cole plots can be obtained using a nonisothermal method.

From the Cole–Cole interactions presented in Figure 4, it is noted that the EVA sample show a flattened curve when compared to nanocomposites followed by the 30B, Na^+ and 15A nanocomposites, respectively. So, it is clear that the samples containing the nanofillers promote a heterogeneous relaxation process when compared to the neat EVA.

Oscillatory rheometry

Figure 5 shows the storage (G') and loss (G'') moduli obtained by oscillatory rheometry at a preset temperature of 160°C. It can be observed that G'' has higher values in comparison to G', since the viscous response related to the energy dissipation is predominantly through the higher energy state.[23] Thus, in relation to pure EVA and EVA/Na^+ it is clear that at low frequencies the increase in the modulus is gradual. This is due longer time intervals favors the material response to the orientation in the direction of the force applied. At higher frequencies, the time interval is shorter and the polymer chains are not able to dissipate the energy applied by the mechanical stress, showing a linear behavior. Thus, by incorporation of the sodium clay, it was noted that this nanofiller does not cause significant effects in relation to the degrees of freedom of the polymeric chains of the EVA matrix, corroborating the results found in the literature.[24]

In relation to the nanocomposites containing the15A and 30B clays, an increase in the G' and G'' moduli is evident as well an approximation of the

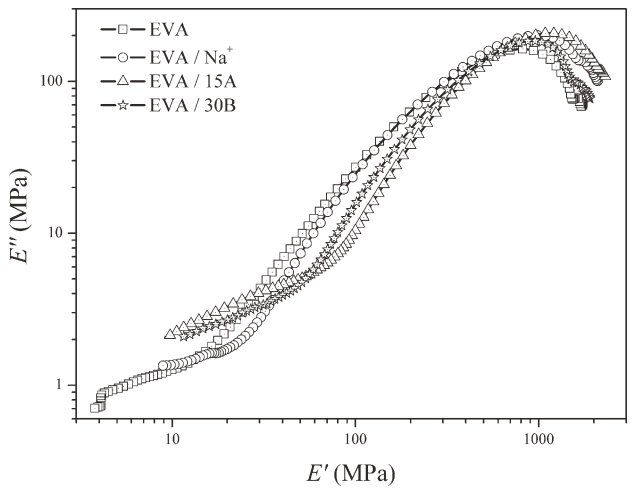

Figure 4 Cole–Cole model obtained for the neat EVA and the nanocomposites studied.

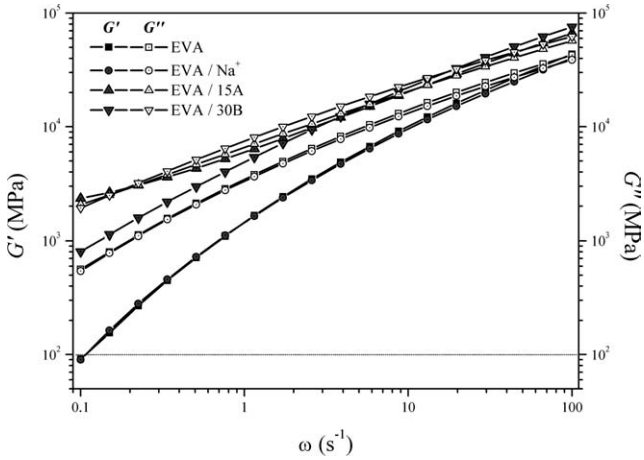

Figure 5 Storage (G') and loss (G'') moduli for the neat EVA and the nanocomposites obtained by oscillatory rheometry.

values for the two moduli. This is indicative of a decreasing in the loss factor and an increasing in the capacity to store higher energy in the system. However, for lower frequencies, the 30B nanoclay shows a linear increasing in the G' values. The 15A nanocomposite shows moduli values higher than those of 30B and as the frequency is increased, these values stabilize. This phenomenon, when associated with the type of surfactant used, can be related to the existence of a disentanglement point of the EVA chains and the chain segments of the 15A nanoclay. The 30B nanoclay, by having small number of carbon segments at the surface of the platelets, shows a linear trend for the increase in the G' modulus as the frequency increased. However, the higher stability observed with the increase in the moduli for both modified nanoclays may be due to the physical interaction between the chain segments of the 15A clay and the OH terminals, as well an interaction of the acetate groups of the 30B nanofiller and the EVA matrix.

These interactions corroborate the results obtained from the DMA analysis, since the increase in the T_g values and the reduction in the tan δ height peak are indicative of higher homogeneity of the nanoclays, demonstrating that the nanofillers influence the viscoelastic properties in the solid and molten state.

Viscoelastic functions

The most important difference between the solid and the molten state is the molecular scale in relation to relaxation processes.[25] In the solid state, the molecular relaxation is characterized by variations in the heat capacity (ΔC_p) and, consequently, an increase in the entropy (ΔS). Since the energetic barrier has a great influence in the solid state, the molecular mobility is extended in different relaxation processes.[16]

By increasing the internal energy, the relaxation phenomenon tends to propagate through cooperativity effects, however, these effects are dependent on the complexity of the polymeric structure. The main relaxation processes in the solid state are observed at and below the glass transition temperature (T_g). These transitions originate from molecular movement of groups or parts of side groups.[16] At temperatures above the T_g, the macromolecules are found in a state of higher internal energy and a considerable change in the free volume promotes a change of the physical state with entanglement or packing of the chains, leading to a considerable reduction in the viscosity of the material. This phenomenon is known as a first-order transition and is characteristic of the molten state.[26] In this state, the free volume is large and the chains have a high number of degrees of freedom, which is sufficient to create a random conformation through a higher energy state.[16,27] As the molten state is a process of molecular relaxation,[26] it is interesting to investigate how the relaxation process occurs with the presence of these nanoclays. In this regard, from the G' and G'' data as a function of the frequency variation, observed in Figure 6, it is possible to obtain the relaxation and retardation spectra through the relation proposed by Rhots *et al*.[8] using the software of nonlinearization regression (NLREG) according to eqs. (1) and (2):

$$G'(\omega) = G_\theta + \int_{-\infty}^{\infty} H(\tau)\frac{\omega^2\tau^2}{1+\omega^2\tau^2} d\ln\tau \quad (1)$$

$$G''(\omega) = \int_{-\infty}^{\infty} H(\tau)\frac{\omega^2\tau^2}{1+\omega^2\tau^2} d\ln\tau \quad (2)$$

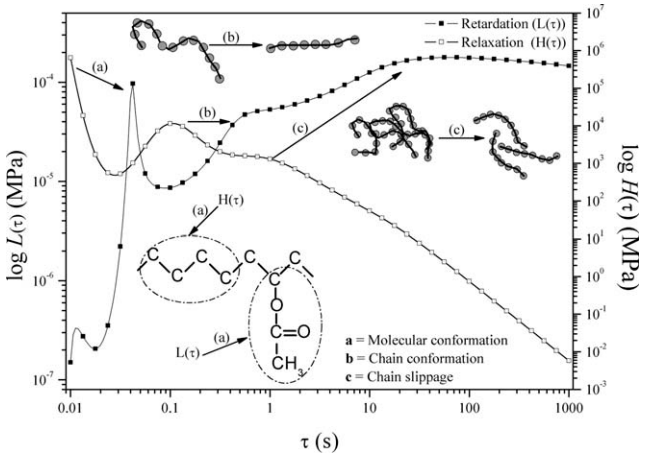

Figure 6 Relaxation spectra calculated by oscillatory rheometry measurements for the neat EVA and the nanocomposites studied.

where G_θ is the equilibrium modulus, $H(\tau)$ is a function of the relaxation spectrum, and τ is the relaxation or retardation time.

The relaxation spectrum is the result of an infinite sum of Maxwell elements that describe the mechanical behavior of the elastic portion of the polymer and its ability to store energy[8,9,16] [eq. (3)]. Estimates of the retardation spectrum are obtained through the inter-relationships of the spectra described by Ferry and results from the infinite sum of Voigt elements that are responsible for any portion of the viscous polymer[16] [eq. (4)].

$$H(\tau) = \frac{L(\tau)}{\left[J_g + \int_{-\infty}^{\infty} \frac{L(\tau)}{(1-\tau)/\tau} d \ln \tau - \frac{\tau}{\eta_0}\right]^2 + \pi^2 L(\tau)^2} \quad (3)$$

$$L(\tau) = \frac{H(\tau)}{\left[G_\theta - \int_{-\infty}^{\infty} \frac{H(\tau)}{\tau/(\tau-1)} d \ln \tau\right]^2 + \pi^2 H(\tau)^2} \quad (4)$$

where J_g is the instantaneous compliance, η_0 is the zero-shear viscosity, and G_θ is the equilibrium modulus.

Figure 6 shows the relaxation spectra obtained using the NLREG algorithm for the samples studied. As can be observed there is the appearance of two distinct relaxation peaks at $\tau \approx 0.1$s and $\tau \approx 1$s for the EVA sample.

According to Matsuoka,[25] in the molten state there are three characteristic relaxation stages, the unkinking stage associated with chain conformation (Stage 1), chain slippage (Stage 2) due to the higher number of degrees of freedom and the free volume, and correlated blob slippage (Stage 3).

Therefore, it can be assumed that the distribution of relaxation times in the first peak is dependent on the complex structure of the EVA polymer (the branching of the ethylene segments and the physical interactions between the VAc polar groups presented in EVA (Stage 1) contributing to this). The second relaxation phenomenon can be associated with the distribution of relaxation times that extends with the slipping and entanglement of long polymeric chains (Stages 2 and 3). Consequently, there is a delay in the relaxation related to the distribution of the molecular weight and thus, the type and size of the chain. Also, with incorporation of the sodium clay, a distinct behavior in relation to the relaxation phenomenon were not observed, suggesting that the chains have the same degrees of freedom for the relaxation phenomenon when compared with the pure EVA matrix.

However, when the 15A and 30B nanoclays were incorporated, the appearance of a third relaxation phenomenon was noted. For the 30B nanocomposite, the third relaxation peak is found at $\tau \approx 10$s and for the nanocomposite containing 15A, at $\tau \approx 30$s. For the two relaxation phenomena, no significant changes occurred in the distribution of the relaxation times, suggesting that the first and second relaxation stages are not affected by the presence of the nanoclays. From these results, it can be assumed that the third relaxation process is related to restriction in the mobility of individual segments of the EVA chain between the galleries of the modified clays (related to correlated blob slippage).

It is important to mention that, in the case of an intercalated morphology, it is possible that the slippage of the chains along the flow be impeded, since the platelets inhibit the chain movement. This phenomenon explains the higher shift of the third relaxation phenomenon observed in the nanocomposites containing the 15A clay, suggesting a more intercalated system in relation to the 30B nanocomposite. This description is consistent with the appearance of three distinct peaks in the XRD analysis (Fig. 1). Chaudhary et al.[7] also described this characteristic when there is intercalation of the polymer chains between the galleries of the clay.

The retardation time $L(\tau)$ describes the viscous portion of the system through the sum of infinite Voigt elements.[16,28] The shape of these spectra is indicative of the inhibited mobility of the segments in the molten state. The results obtained for the EVA and the nanocomposite containing Na^+ are represented in Figure 7 and show a similar trend for all the samples studied. For these samples three distinct retardation characteristics at $\tau \approx 0.04$, 0.5, and 8 s were observed. Probably, the first retardation peak is originated of a relaxation phenomenon that does not appear in the range of frequency studied. It can be noted that for the relaxation spectra of the EVA and Na^+ nanocomposites, the second and third relaxation stages were considered to be overlapped

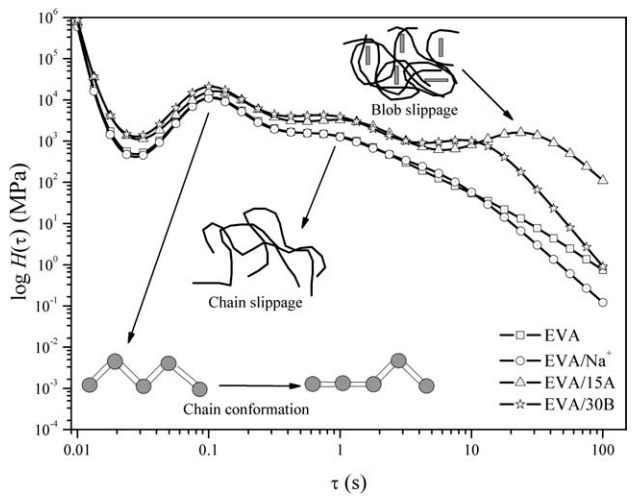

Figure 7 Retardation spectra calculated by oscillatory rheometry measurements for the neat EVA and the nanocomposites studied.

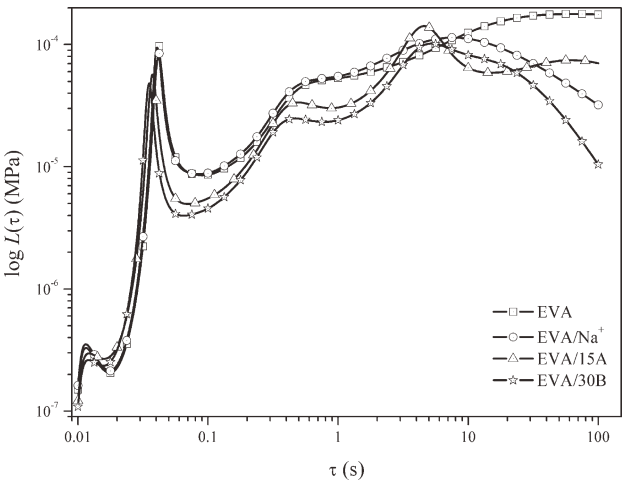

Figure 8 Proposed scheme for understanding of the relaxation and retardation phenomena related to the nanocomposites studied.

presenting a single relaxation phenomenon. Also, it can be seen in Figure 7 that the separation of the Stages 2 and 3 is evident, since the viscous portion related to the blob slippage shows a delay in the relation to an individual segment. On comparing the spectra obtained for the nanocomposites containing the 15A and 30B nanoclays, it is possible to observe the shift in the retardation peaks to lower times and the appearance of a fourth retardation peak for the nanocomposites containing the 15A nanoclay. The reduction in the retardation time, in this case, may be inhibited by a strong physical interaction between the segments of the chains and the type of surfactant present on the surface of the modified nanoclays. In addition, since the relaxation times become more heterogeneous over time, it is expected that these phenomenon will be noted for lower values. This occurs since there is proportionality between the elastic and plastic deformation, i.e., higher elastic deformation for $H(\tau)$ leads to a lower and less pronounced effect on the plastic deformation for $L(\tau)$.[16,26] Also, this corroborates with the approximation of the moduli, as observed in Figure 7. In relation to the appearance of a fourth retardation phenomenon, this may be due to physical interaction between the surface of the 15A nanoclay that forces the shift and the orientation of the platelets of the intercalated clay. The fourth peak is probably, a consequence of the inhibited mobility of the individual chain segments in the polymeric chains, due to entanglement with the segments of the chains of the clay.

Figure 8 represents the shift of the retardation spectrum in relation to the relaxation spectrum. It can be observed that the first retardation phenomenon (depicted as (a)) probably is provided from an earlier relaxation phenomena not presented in the range of frequency studied (Grassia and D'amore[29] related that the relaxation phenomena should occur before the corresponding one] and it is related to the molecular conformation of the EVA chains. As the time prolongs, there is chain conformations (showed as (b)) and it is observed a less pronounced retardation peak in relation to the first peak due a broader relaxation times distribution. Finally, occurs the chain slippage (showed as (c)) of the molecular segments and the presence of the peak is less intense than the other ones.

Transmission electron microscopy (TEM)

Figure 9 shows the TEM micrographs for the nanocomposites studied at a processing speed of 400 rpm. The nanocomposite containing the Na^+ clay shows characteristic of microcomposite agglomerates.[24] In relation to the nanocomposite 15A, the presence of intercalated structures (that are visually observed from the dispersed lower platelets) in the EVA matrix was verified. The confirmation of this intercalated morphology corroborates with the inhibited chain relaxation (Fig. 6) and the appearance of a fourth retardation phenomenon (Fig. 7). Besides, the movement of chain segments hindered by the EVA chain entanglement between the galleries of the 15A clay facilitates the formation of an intercalated structure. With the incorporation of 30B nanofiller, the predominant morphology observed was the exfoliated, corroborating with the viscoelastic properties observed in this study.

Since the platelet separation produces more percolated clay in the matrix, one of the factors related to the strong interaction of the 30B is the presence of OH terminals in the surfactants used to modify the surface of the clay. According to Marini et al.,[4] clays modified with polar tensoactives turn the exfoliation more efficient.

Also, for the nanocomposites containing 15A and 30B nanofiller (intercalated and exfoliated morphologies, respectively) the presence of other morphological characteristics can be observed. This is due some factors like the polar surfactants (more compatible with hydrophilic polymers)[4,7] and the polarity[5] that contributes for the formation of determinated morphology. Also, depending the morphology obtained, there are modifications in the T_g values due the formation of a more rigid and homogeneous system. Furthermore, the nanocomposite containing the 15A clay has higher flow stability, reflecting strong physical interactions due to the chain entanglements of 30B containing OH terminals.

CONCLUSIONS

In this study, the performance of different nanocomposites obtained with distinct clays was evaluated.

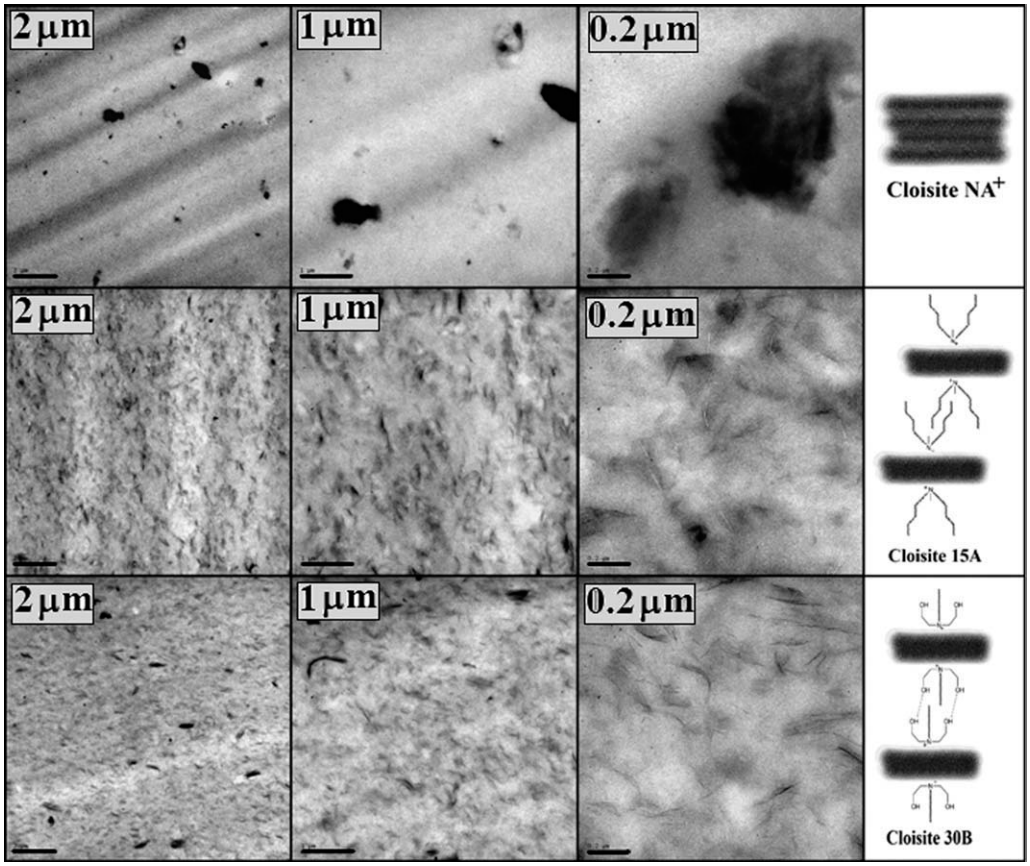

Figure 9 Transmission electron microscopy (TEM) obtained for the nanocomposites.

According DMA results, higher values for the storage and loss moduli were observed for the sample containing the organophilic clay 15A. Also, for this nanocomposite the peak height and peak width at half-height showed lower values.

In the oscillatory rheometry analysis, the nanocomposites containing the organophilic clays showed higher values in the properties measured. The relaxation spectra showed two distinct peaks for EVA and the NA^+ nanocomposites, and three peaks for the 15A and 30B nanocomposites. In relation to the retardation spectra, for the sample 15A the appearance of a fourth peak was noted.

The shift of the third relaxation and retardation spectra for 30B and 15A nanocomposites were associated to the molecular restraint of the EVA chains in the dispersed clays. Besides, it was possible relate that the intercalated clay interferes of a more pronounced way in the chain slippage than 30B clay nanocomposite.

XRD and TEM analyses showed a microcomposite formation for the NA^+ sample, a more intercalated system for the sample containing the nanoclay 15A and a more exfoliated system for the 30B nanocomposite.

Finally, TEM analyses are in agreement with the retardation and relaxation spectra, demonstrating that the intercalated morphology promotes more restraints in the molecular motion than the exfoliated morphology obtained by 30B incorporation.

References

1. Ray, S. S.; Okamoto, M. Prog Polym Sci 2003, 28, 1539.
2. He, H.; Ma, Y.; Zhu, J.; Yuan, P.; Qing, Y. Appl Clay Sci 2010, 48, 67.
3. Riva, A.; Zanetti, M.; Braglia, M.; Camino, G.; Falqui, L. Polym Degrad Stabil 2002, 77, 299.
4. Marini, J.; Branciforti, M. C.; Lotti, C. Polym Adv Technol 2010, 21, 417.
5. Zhang, W.; Chen, D.; Zhao, Q.; Fang, Y. Polymer 2003, 44, 7953.
6. La Mantia, F. P.; Dintcheva, N. T. Polym Test 2006, 25, 701.
7. Chaudhary, D. S.; Prasad, R.; Gupta, R. K.; Bhattacharya, S. N. Polym Eng Sci 2005, 45, 889.
8. Roths, T.; Marth, M.; Weese, J.; Honerkamp, J. J Comput Phys Commun 2001, 139, 279.
9. Dal Castel, C.; Bianchi, O.; Oviedo, M. A. S.; Liberman, S. A.; Mauler, R. S.; Oliveira, R. V. B. Mater Sci Eng C 2009, 29, 602.
10. Weese, J. Comput Phys Commun 1993, 77, 429.
11. Gupta, R. K.; Pasanovic-Zujo, V.; Bhattacharya, S. N. J Non-Newtonian Fluid Mech 2005, 128, 116.
12. Yamaki, S. B.; Prado, E. A.; Atvars, T. D. Z. Eur Polym J 2002, 38, 1811.
13. Hameed, N.; Sreekumar, P. A.; Francis, B.; Yang, W.; Thomas, S. Compos A Appl Sci Manufact 2007, 38, 2422.

14. Pothan, L. A.; Thomas, S.; Groeninckx, G. Compos A Appl Sci Manufact 2006, 37, 1260.
15. Cowie, J. M. G. Polymers: Chemistry and Physics of Modern Materials; Intertext Books: UK, 1973.
16. Ferry, J. D. Viscoelastic Properties of Polymers; Wiley: New York, 1980.
17. Roudaut, G.; Poirier, F.; Simatos, D.; Le Meste, M. Rheol Acta 2004, 44, 104.
18. Ornaghi, J. R. H. L.; Bolner, A.; Fiorio, R.; Zattera, A. J.; Amico, S. C. J Appl Polym Sci 2010, 118, 887.
19. Eker, S.; Bozdenir, S. J Non Cryst Solids 2010, 356, 553.
20. Hodge, I. M. Biophys J 2006, 91, 993.
21. Qazvini, N. T.; Mohammadi, N. Polymer 2005, 46, 9088.
22. Shaw, M. T.; Macknight, W. J. Introduction to Polymer Viscoelasticity; Wiley: New Jersey, 2005.
23. Hong Mei, Y.; Qiang, Z.; Miao, D. Chem Res Chin Univ 2006, 22, 651.
24. Paul, D. R. Polymer 2008, 49, 3187.
25. Matsuoka, S. Relaxation Phenomena in Polymers; Hanser Publishers: New York, 1992.
26. Eisele, U. Introduction to Polymer Physics; Springer-Verlag: New York, 1990.
27. Strobl, G. R. The Physics of Polymers; Springer-Verlag: New York, 1996.
28. Pistor, V.; Lizot, A.; Fiorio, R.; Zattera, A. J. Polymer 2010, 51, 5165.
29. Grassia, L.; D'Amore, A. J Rheol 2009, 53, 339.